Endothelial eNAMPT drives EndMT and preclinical PH: rescue by an eNAMPT-neutralizing mAb

Mohamed Ahmed[1], Nahla Zaghloul[1], Prisca Zimmerman[1], Nancy G. Casanova[2], Xiaoguang Sun[2], Jin H. Song[2], Vivian Reyes Hernon[2], Saad Sammani[2], Franz Rischard[2], Olga Rafikova[2], Ruslan Rafikov[2], Ayako Makino[2] (iD), Carrie L. Kempf[2], Sara M. Camp[2] (iD), Jian Wang[2,3], Ankit A. Desai[2], Yves Lussier[2], Jason X.-J. Yuan[2] (iD) and Joe G.N. Garcia[2,3] (iD)

[1]Department of Pediatrics, University of Arizona Health Sciences, Tucson, AZ, USA; [2]Department of Medicine, University of Arizona Health Sciences, Tucson, AZ, USA; [3]State Key Laboratory of Respiratory Disease, Guangdong Key Laboratory of Vascular Disease, The First Affiliated Hospital of Guangzhou Medical University, Guangzhou, Guangdong, China

Abstract

Pharmacologic interventions to halt/reverse the vascular remodeling and right ventricular dysfunction in pulmonary arterial hypertension (PAH) remains an unmet need. We previously demonstrated extracellular nicotinamide phosphoribosyltransferase (eNAMPT) as a DAMP (damage-associated molecular pattern protein) contributing to PAH pathobiology via TLR4 ligation. We examined the role of endothelial cell (EC)-specific eNAMPT in experimental PH and an eNAMPT-neutralizing mAb as a therapeutic strategy to reverse established PH. Hemodynamic/echocardiographic measurements and tissue analyses were performed in Sprague Dawley rats exposed to 10% hypoxia/Sugen (three weeks) followed by return to normoxia and weekly intraperitoneal delivery of the eNAMPT mAb (1 mg/kg). WT C57BL/6J mice and conditional EC-cNAMPT$^{ec-/-}$ mice were exposed to 10% hypoxia (three weeks). Biochemical and RNA sequencing studies were performed on rat PH lung tissues and human PAH PBMCs. Hypoxia/Sugen-exposed rats exhibited multiple indices of severe PH (right ventricular systolic pressure, Fulton index), including severe vascular remodeling, compared to control rats. PH severity indices and plasma levels of eNAMPT, IL-6, and TNF-α were all significantly attenuated by eNAMPT mAb neutralization. Compared to hypoxia-exposed WT mice, cNAMPT$^{ec-/-}$ KO mice exhibited significantly reduced PH severity and evidence of EC to mesenchymal transition (EndMT). Finally, biochemical and RNAseq analyses revealed eNAMPT mAb-mediated rectification of dysregulated inflammatory signaling pathways (TLR/NF-κB, MAP kinase, Akt/mTOR) and EndMT in rat PH lung tissues and human PAH PBMCs. These studies underscore EC-derived eNAMPT as a key contributor to PAH pathobiology and support the eNAMPT/TLR4 inflammatory pathway as a highly druggable therapeutic target to reduce PH severity and reverse PAH.

Introduction

The pathobiology of pulmonary arterial hypertension (PAH) is complex and pharmacologic therapies to stabilize or reverse established PAH remains an unmet need. Our human PAH and experimental PH studies implicated inflammatory cascade activation[1,2] and the participation of nicotinamide phosphoribosyltransferase, a cytozyme exhibiting intracellular NAD-regulatory activities (iNAMPT) and extracellular cytokine-like properties (eNAMPT).[3,4] We have determined eNAMPT as the essential contributor to PH severity,[4] with plasma eNAMPT levels linked to clinical indices of PAH severity including RV dysfunction.[4] Circulating eNAMPT functions is a

Corresponding author:
Joe G.N. Garcia, The University of Arizona Health Sciences 1230 N Cherry Ave, Room 441, Tucson, AZ 85719, USA.
Email: skipgarcia@email.arizona.edu

damage-associated molecular pattern protein (DAMP) via TLR4 ligation and NF-κB activation[5,6] with eNAMPT neutralization (polyclonal antibody) attenuating NF-κB activation, vascular remodeling, and preclinical PH hemodynamic alterations.[4]

The current study substantially extends prior reports and validates eNAMPT as an attractive PAH therapeutic target utilizing a novel humanized eNAMPT-neutralizing mAb to successfully reverse hypoxia/Sugen-induced rat PH severity and inflammation. We have shown NAMPT to promote endothelial cell (EC) and smooth muscle cell survival and to induce endothelial-to-mesenchymal transition (EndMT), a process that influences experimental PH severity. Utilizing $cNampt^{ec-/-}$ mice, we now directly highlight lung EC-derived eNAMPT as a major contributor to the development of EndMT. In biochemical and genomic studies, the eNAMPT mAb potently rectified dysregulated biological signaling pathways in lung tissues from rats with hypoxia/Sugen-induced PH and in PBMCs from human PAH subjects (Toll-like receptor/NF-κB, MAP kinase family, Akt/mTOR). The eNAMPT mAb reduced SNAI1 expression, an EndMT-inducing protein, consistent with known regulation of EndMT by the Akt/mTOR signaling pathway.[4,7,8] These studies confirm EC-derived eNAMPT as a key contributor to PAH pathobiology and support the eNAMPT/TLR4 inflammatory pathway as a druggable target to prevent PAH development and reverse established PAH.

Materials and methods

Reagents

All reagents were purchased from Sigma-Aldrich (St. Louis, MO), unless otherwise noted. Antibodies immunoreactive against p-NFkB, pp-ERK, pp-p38, pp-JNK, mTOR (cat #2972S), Rictor (rabbit mAb 53A2, cat #2114S), phospho-NF-kB p65 (Ser536, 93H1 Rabbit mAb, cat #3033S), phospho-Akt (Thr308, rabbit mAb, 244F9, cat #4056S), and phospho-Akt (Ser473) antibody duet (cat # 8200S) were all purchased from Cell Signaling Technologies (Danvers, MA). Antibodies immunoreactive against β-actin from Invitrogen (Carlsbad, CA). Goat, rabbit, and mouse secondary antibodies were purchased from Life Technologies (Waltham, MA). Human PBEF/Visfatin Biotinylated Antibody (cat #BAF4335) was purchased from R&D systems; Ultra Streptavidin-HRP (cat #N504) from ThermoFisher Scientific; Actin-HRP (cat #A3854-200UL) from Sigma-Aldrich. Peroxidase AffiniPure Goat Anti-Mouse IgG (H+L) (cat# 102646-170) and Anti-IgG (H+L) Goat Polyclonal Antibody (Horseradish Peroxidase) (cat #102645-188) and IgG for use as controls were obtained from Jackson ImmuneResearch (West Grove, PA). Goat anti-human NAMPT pAb was custom-generated by immunizing goats against the full length rhNAMPT protein as we previously described.[9,10] The eNAMPT-neutralizing humanized mAb, ALT-100, was provided by Aqualung Therapeutics Corporation (Tucson, AZ) and was generated from murine eNAMPT-neutralizing mAbs as we have previously described.[10]

Human PAH cohort

Blood for PBMC retrieval was obtained from six adult (age ≥ 18 years) patients with World Health Organization (WHO) Group I PAH who were prospectively recruited from our University Pulmonary Hypertension Registry. Phlebotomy was performed on all subjects to collect plasma samples. Medical record data were collected including demographic and clinical data on all subjects. All subjects provided informed written consent to participate in this study with the approval by the institutional review board (IRB# 1312168664R008).

Study animals

Adult Sprague Dawley male rats (∼200 g) (Jackson Laboratories, Bar Harbor, ME) were used to develop PAH hypoxia/Sugen model. All rats were housed under standard conditions (12 h light–dark cycle, 25–27°C, ∼40% humidity) in autoclaved micro-isolator cages with free access to food and water throughout the duration of the experiments. All animal care procedures and experiments were approved by the Institutional Animal Care and Use Committee.

In addition, in vivo experiments, we utilized wild-type male C57BL/6J mice (8–12 weeks, Jackson Laboratories, Bar Harbor, ME), $Nampt^{+/-}$ mice on a C57BL/6 background, and EC-specific conditional Nampt knockout mice $(cNampt^{ec-/-})$ on a mixed 129/B6 background along with their littermate $Nampt^{fl/fl}$ as controls as we have previously described.[3,9,10] $cNampt^{ec-/-}$ mice were generated by crossing floxed Nampt mice $(Nampt^{fl/fl})$ with tamoxifen-inducible EC-specific Cre transgenic mice (Tek-Cre/ERT2-1Soff)[11] with backcrossing with floxed homozygous Nampt mice as we previously described.[10] After the final dose of tamoxifen, a two-week minimal wait period was implemented before the utilization of $cNampt^{-/-}$ mice for experimentation. EC-specific KO mice carrying the Nampt flox transgene did not display discernible differences in phenotypic traits (growth rate, fecundity, and fertility) compared to their wild-type littermates or wild-type mice.[10] Similarly, Nampt flox mice crossed with the Tek-Cre/ERT2 Cre mice to generate the conditional Nampt KO line did not exhibit phenotypic differences from either littermates or parental strains, both before and after tamoxifen injections.[10]

Hypoxia/Sugen-induced rat model of PH

A rat model of hypoxia/Sugen-induced PH was used as we have previously described [2,3,12] and approved by the Ethics and Animal Care Committee of our University. Briefly, chronic PH was accomplished by exposing Sprague Dawley male rats (9–11 weeks old) to hypoxia 10% and

intraperitoneal administration (20 mg/kg body weight per dose) of the vascular endothelial receptor (VEGF) blocker SU5416 (Sugen; Sigma, St. Louis, MO). Sugen was suspended within a mixture of 0.5% carboxy methyl cellulose sodium, 0.9% sodium chloride, 0.4% polysorbate 80, and 0.9% benzyl alcohol in deionized water. Following three weeks of hypoxia exposure, all animals were returned to housing in room air (weeks 4 through 6) with 50% of the hypoxic rat group receiving IP PBS and 50% of hypoxias-exposed rats treated with the humanized eNAMPT-neutralizing mAb, (1 mg/kg, IP, twice weekly for total of six doses). Echocardiographic studies and hemodynamic measurements were performed after a total of six weeks of study.

Hypoxia-induced mouse model of PH

Adult male wild-type C57B6 mice (WT), heterogenous knockout ($Nampt^{+/-}$) and conditioned KO ($cNampt^{ec-/-}$) mice, were housed in hypoxic chamber (FiO$_2$ 10%) for three weeks. All studied mice groups were subjected to echocardiographic studies before and after hypoxia exposure as well as hemodynamic studies after three weeks of hypoxia exposure.

Echocardiographic studies

Echocardiography was performed using a Vevo 3100 High Resolution Imaging System (Visual-Sonics, Toronto, Canada) with an MX550D (mouse) or MX250 (rat) scan head designed for rodent cardiac imaging. Following anesthetic induction in 3% isoflurane, animals were placed in a supine position on a heated platform to maintain body temperature of 37°C. Anesthesia was maintained with 1.5–3% isoflurane (USP, Phoenix) in 100% oxygen and echo images collected and stored as digital cine loops for off-line calculations. Standard imaging planes, M-mode, Doppler, and functional calculations were obtained according to American Society of Echocardiography guidelines. A short axis M-mode cine loop was recorded at the level of the papillary muscles to assess chamber dimensions (LV systolic and diastolic dimensions) posterior wall thickness (PWT), and cardiac function via fractional shortening (% FS). Doppler imaging was obtained from an apical four-chamber view to assess LV filling and tissue velocity of the septal mitral valve annulus. A modified parasternal long axis view was used to assess right ventricle (RV) free wall thickness and RV chamber diameter. A short axis view at the level of RVOT was used to assess pulmonary artery diameter (B-mode) and flow (PW Doppler). Ejection fraction measurements were estimated from the RVP waveform based upon the concept of single beat quantification of RV: pulmonary arterial coupling.[13,14]

Hemodynamic studies

RT ventricular pressure assessment. This was evaluated at 3, 7, 11, and 14 weeks' post hypoxia exposure as we have described[15] utilizing a Millar catheter inserted in right jugular vein and then into the right ventricle. Right ventricular systolic pressure (RVSP) was measured and recorded using a computerized hemodynamic recording system (HAEMODYN, Harvard Apparatus, MA, USA). *RV/S + LV ratio:* Hearts were removed, dissected, and weighed for calculation of different of cardiac indices. The heart weights were be expressed as a ratio of the weight of the right ventricle to that of the septum plus left ventricle (RV/S + LV), or the right ventricle mass (right ventricle/weight – RV/W), was expressed the ratio of the weight of the right ventricle to the weight of the animal.[3,4]

Quantification of microvessel density and vascular wall thickness. The left lung was perfused with 4% paraformaldehyde (PFA), inflated by infusion of 4% PFA at a constant pressure of 25 cm H$_2$O through a cannula inserted in the trachea, fixed in 4% PFA overnight at 4°C and then embedded in OCT, Subsequently 5-μm-thick sections were taken and stained with hematoxylin and eosin (H&E) images of individual pulmonary arteries were captured using a digital camera, mounted on a light microscope, and linked to a computer. Microvessel density was quantified by counting the percentage area of positive pixels per image with at least 21 images per sample (5 animals, 3 samples per animal, and 7 sections per sample as described previously).[15]

Vascular wall thickness. This was measured using a Zeiss Axiovert 200M light microscope – CCD camera AxioCam (mRm) color camera and expressed as the percentage of total vessel size. Percent wall thickness was calculated as (2× wall thickness)/external diameter. 100%. External diameter and internal diameter of 50 alveolar vessels (with an external diameter of 100–200 μm) per animal were determined and recorded by an independent investigator blinded to the treatment regimen. The ratio of vessel wall area to total area (WA%) and the ratio of pulmonary arteriole wall thickness to vascular external diameter (WT%) were measured using Zeiss axial program of three random wall sections.

Lung histology, immunohistochemistry, and Image J quantification

To assess alterations in the lung tissue morphology, lungs collected from sacrificed rats and mice were fixed in 10% Neutral Buffered formalin for a minimum of 48 h, embedded in paraffin, sectioned, mounted onto slides, and stained with hematoxylin-eosin (H & E).[10]

NAMPT immunohistochemistry evaluation (IHC)

IHC staining for NAMPT (5 μm sections) was performed using the avidin-biotin-peroxidase method to visualize lung tissue expression of NAMPT with anti-NAMPT (Bethyl Laboratories, Montgomery, TX) or with a matched protein concentration (1 μg/ml) of rabbit IgG (Vector Labs, Burlingame, CA). Slides were deparaffinized and rehydrated to distilled water. Sections were ringed with an ImmunoPen rinsed in TBS, blocked for endogenous peroxidase using freshly prepared 0.5% hydrogen peroxide, 20 min, washed, protein block (Vector Labs) for 1 h, followed by avidin D and biotin block (Vector Labs), all at room temperature. Slides were incubated in primary or IgG isotype control, overnight at 4°C with humidity. After washing, biotinylated secondary was applied for 1 h, washed and incubated with avidin-biotin complex (Vector Labs) 40 min, all at room temperature. The protein was visualized using DAB plus nickel (Vector Labs), 4 min, rinsed in tap water and counterstained with Mayers hematoxylin (Newcomer Supply, Middleton, WI) 30 s, washed in water, bluing reagent (Richard-Allan Scientific, San Diego CA) 10 s, washed in water, dehydrated, cleared, and cover-slipped with DPX. Routine H&E slides were prepared using Richard-Allan hematoxylin, clarifier, bluing reagent, and eosin.[10]

Plasma biomarker measurements

For measurements of plasma levels of eNAMPT, IL-6, and TNF-α, a meso-scale ELISA platform was utilized (Meso Scale Diagnostics, Rockville, MD) as we have described.[5,10] Each biotinylated antibody, specific for each analyte, was diluted in the coating buffer to a concentration of 10 μg/ml. A volume of 200 μl of diluted antibody was next mixed with 300 μl of a different linker for each analyte and vortexed. After 30 min RT incubation, the reaction was stopped with 200 μl of free biotin solution. Then, 600 μl of this 10× U-PLEX linked biotinylated antibody solution was added to a tube and mixed. The volume was supplemented with Stop and 50 μl of coating solution added to each well in 96 well plate and incubated for 1 h at 800 r/min shaking at room temperature. After washing three times, the plate was supplemented with 25 μl of diluent and 25 μl of calibrator or samples/standards to each well. The plate was incubated for 1 h at 800 r/min at RT. After washing three times with TBS-T, the plate was supplemented with 50 μl/well of 1× detection antibody solution to each well before being again incubated for 1 h at 800 r/min shaking at RT. After washing three times with TBS-T the plate was supplemented with 150 μl/well of 2× Read Buffer T. The plate was finally detected in the imager and the absolute concentration values were calculated based on standards.[10]

Western blotting and biochemical tissue analyses

Western blotting of proteins within rat lung tissue homogenates was performed as we have previously reported.[10] Snap-frozen lung tissues were homogenized in RIPA buffer (50 mmol/L Tris-HCl pH 7.4, 150 mmol/L NaCl, 0.5% sodium deoxycholate, 0.1% SDS, 1% NP-40, 5 mmol/L EDTA) supplemented with complete protease/phosphatase inhibitor cocktail (Cell Signaling Cat #5872S) using tissue grinder with glass pestles (VWR Cat #26307-606). After centrifugation (15,000 g for 20 min at 4°C), protein concentration of homogenates was determined by Bio-Rad DC protein assay (cat #5000112). Following incubation 5 min at 90°C in loading buffer, aliquots containing equal amounts of protein (25–30 μg) were subjected to sodium dodecyl sulfate polyacrylamide gel electrophoresis (SDS-PAGE). Subsequently, proteins were transferred to PVDF membranes and probed with specific primary antibodies by horseradish peroxidase-conjugated secondary antibodies. Proteins were visualized using an ECL system (Pierce West Pico cat #34580) and ChemiDoc MP imaging system (Bio-Rad). Densitometric analysis was performed using Bio-Rad Image Lab 6.01 software by normalizing the levels of proteins to b-actin expression. The levels of phosphor-proteins were quantified by normalizing the levels to their respective total proteins.[10]

Rat lung tissue and human PBMC RNA sequencing

Rat lung tissue RNA was extracted and RNA QC assessed via the Aligient 2100 Bio analyzer (Agilent RNA 6000 Nano Kit), RIN value, 28S/18S and the fragment length distribution. Following library construct, RNA was sequenced using BGISEQ platform with a sequencing length PE100; averagely generating 15.00 Gb bases per sample with a mapping ration with reference genome of 94.2%, with a total of 20,150 genes identified. Human PBMC RNA was obtained (six PAH subjects, six healthy donors) and sequenced using Illumina NOVASEQ 600 sequencing system and discovery and validation data sets processed separately utilizing NOISeq library [16] to filter genes with low counts (cpm <30) producing 6865 genes for downstream statistical analysis. Human PBMC RNA was extracted and sequenced and bioinformatic analyses conducted. Multiple bioinformatic analytical programs were utilized to identify differentially expressed genes (DEGs) and enriched Gene Ontology (GO) and KEGG pathways.[16-25]

Prioritized differentially expressed genes

RNAseq data were processed with the *NOISeq* library[16,26] in order to filter out the transcripts with low count, specifically with cpm <30. This procedure resulted in 6865 transcripts for downstream statistical analysis. We then utilized the function "*ARSyNseq*"[20] implemented in R package *NOISeq* together with TMM normalization in order to remove the known batch effects in addition to other

hidden and noisy systematic variation. Through the use of function "*voomWithQualityWeights*"[18,19,22] from *LIMMA* package[23,24] the processed RNA count values were transformed for downstream statistical analysis with linear model implemented in *LIMMA* R library. The moderate *t.test* implemented in *LIMMA* was used to derive the transcripts having correlated expression values with phenotypic difference.

Functional biological analyses of transcripts

The Fisher's Exact test followed by false discovery rate (BH method[27]) was utilized to correct for multiple testing and evaluate the over-representation of prioritized transcripts for which the corresponding gene is annotated in each Gene Ontology biological processes (GO BPs). Using information theoretic similarity (ITS) we also unbiasedly identify highly related GOBPs pairs at ITS > 0.7.[28] Using the distance matrix derived from the pairwise ITS values ranging from 0 to 1, the method Ward hierarchical clustering algorithm, which is implemented as default function in R. We finally inferred the distinct of clusters through visual inspection.

Biological interaction network analyses

In order to prioritize genes that biologically interact with one another, we employed the molecular database STRING (Version 11), with the interaction confidence parameter ≥ 0.7.[25]

DEG and gene ontology (GO) and KEGG pathway enrichment analyses

Bioinformatic analyses included calculation of Pearson correlations of all genes expressed to reflect the correlation of gene expression between samples. The HISAT2 and (Hierarchical Indexing for Spliced Alignments of Transcripts) Bowtie2 programs were utilized to align and clean reads to the reference genome and to the reference genes.[17,21,29] DEseq2 algorithms were used to detect DEGs deemed significant with a False Discovery Rate of <0.05 and a Fold Change of 1.5.[30] Enrichment analysis for Gene ontology (GO) classification was performed focused on biological process and pathway classification. STRING database[25] was used to analyze the protein and protein interaction and construct the interaction networks of the DEGs. In addition, "ARSyNseq" within R package NOISeq was utilized. Together with TMM normalization, known batch effects were removed in addition to additional hidden and noisy systematic variation. Through the use of function "voomWithQualityWeights" from LIMMA package, we further made the processed RNA count values ready for downstream statistical analysis with linear model implemented in LIMMA R library and utilized the moderate t-test implemented in LIMMA to derive the genes

having correlated expression values with phenotypic differences.

Data processing and Limma package (version 3.9) in R software was used for performing normalization and log2 conversion for the matrix data of each GEO dataset, as well as for screening DEGs in each dataset. $|\log2FC| \geq 1$ and adjusted p-value < 0.05 were set as the statistically significant criteria for the DEGs. VolcanoPlot function and Heatmap package in R software were applied to visualize the DEGs between the PAH and control groups.

Before GO and KEGG pathway enrichment analysis, VennDiagram package in R software was applied to obtain the CoDEGs in the datasets. GO enrichment analysis includes three terms, such as biological process (BP), molecular function (MF), and cellular component (CC). The Kyoto Encyclopedia of Genes and Genomes database (KEGG) contains genomic, chemical, functional, and metabolic information. The Database for Annotation, Visualization, and Integrated Discovery(DAVID) is commonly used for gene function analysis as an ideal tool.[21] In this study, the GO and KEGG pathway enrichment analyses of the CoDEGs were conducted using DAVID online tools according to a p value of less than 0.05. For PPI network construction, module analysis, and hub genes selection, the STRING database was applied for analyzing protein–protein interactions (PPI).[17] PPI information of the CoDEGs was obtained from the STRING database and was further visualized using Cytoscape 3.6.1 software. The confidence score ≥ 0.7 was set as the cut-off criterion. The network module as part of the PPI network may contain specific biological functions. Therefore, the Molecular Complex Detection (MCODE) plugged-in Cytoscape was applied for selecting notable modules in this PPI network. The advanced options were set as Node Score Cutoff $= 0.2$, Degree cutoff $= 2$, K-Core $= 2$, and maximal depth $= 100$. Finally, the Cytoscape plug-in CytoHubba was applied to select hub genes in this PPI network. The top 10 nodes ranked by MCC were selected and validated.

Statistical analysis

Continuous data were compared using nonparametric methods and categorical data by Chi square test. Where applicable, standard one-way analysis of variance (ANOVA) was used and groups were compared using the Newman-Keuls test. Differences between groups were considered statistically significant when p values were less than 0.05 ($p < 0.05$). Two-way ANOVA was used to compare the means of data from two or more different experimental groups. If significant differences were present by ANOVA ($p < 0.05$), a least significant differences (LSD) test was performed post hoc. Between-group differences were considered statistically significant when $p < 0.05$. Statistical tests were performed using GraphPad Prism version 7.00 for Windows (GraphPad Software, La Jolla California USA).
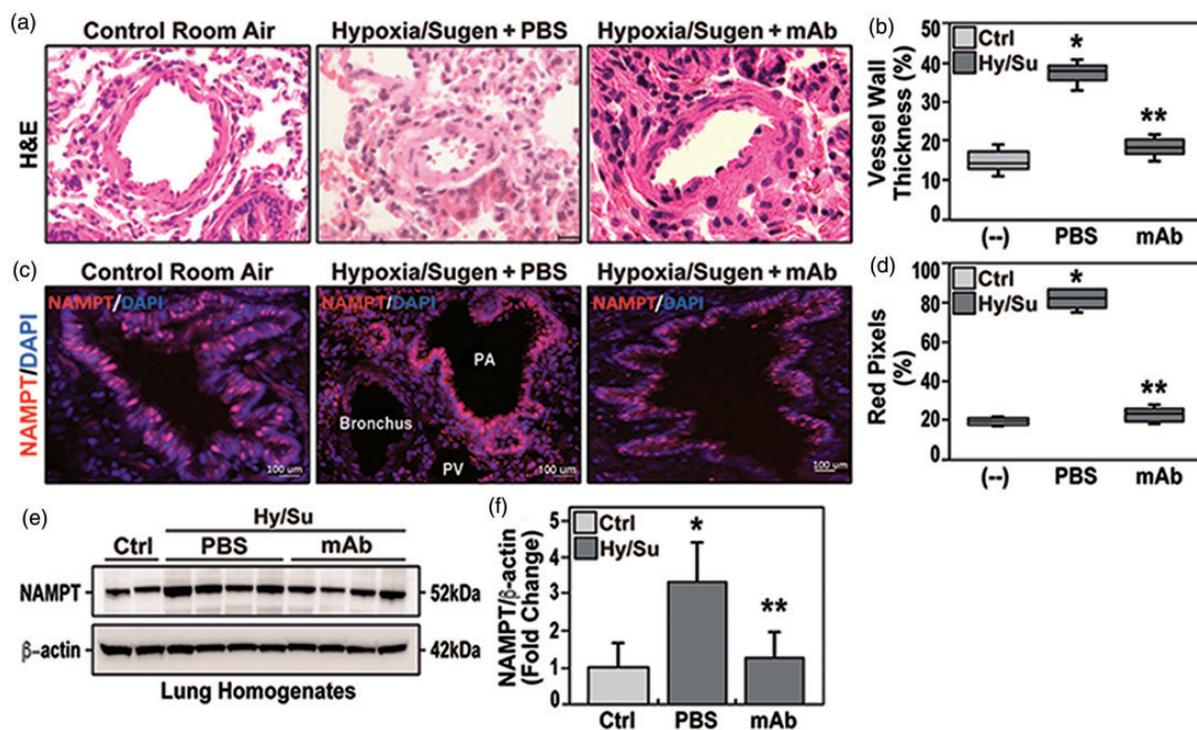
Figure 1. (a) H&E studies in adult Sprague Dawley rats harvested at six weeks exposed to room air (control rats), to hypoxia/Sugen plus PBS beginning at three weeks (three weeks hypoxia exposure, FiO_2 10%), and to hypoxia/Sugen-exposed rats receiving IP delivery of eNAMPT mAb beginning at three weeks (1 mg/kg). Compared to room air-exposed rats, hypoxia/Sugen/PBS-exposed rats displayed significant increases in vessel wall thickness and near obliteration of the intravascular lumen. In contrast, eNAMPT mAb treated hypoxia/Sugen-exposed rats were markedly protected with nearly complete normalization of vessel wall thickness. (b) Qualitative evaluation (boxplots) of vascular wall thickness (VWT) showing a significant reduction of hypoxia/Sugen/PBS-induced increases in VWT in rats receiving the eNAMPT mAb. (c) Immunostaining for NAMPT (Bethyl Laboratories, Montgomery, TX) showed significant NAMPT expression (red signals) in endothelial cells lining the pulmonary vascular wall (size 50–100 μm)in hypoxia/Sugen/PBS-exposed rats compared to eNAMPT mAb-treated, hypoxia/Sugen-exposed rats and RA-exposed control rats. (d) Quantitative evaluation of the percentage of NAMPT pixels in five sections/animal. (e) NAMPT Western blot assay in studied groups (with corresponding densitometric quantification of NAMPT protein levels (Panel f), showing significant reduction in NAMPT expression in eNAMPT mAb-treated, hypoxia/Sugen-exposed rats. N= 5/groups. Bars represents mean ± SE. * $p < 0.05$, ** $p < 0.01$.

Results

eNAMPT neutralization attenuates pulmonary vascular remodeling in the hypoxia/Sugen-induced rat PH model

We utilized the well-validated preclinical Sprague Dawley rat model of PH produced by 10% hypoxia/Sugen[2] to evaluate eNAMPT as a therapeutic PAH target. H&E staining of hypoxia/Sugen lung tissue sections at six weeks demonstrated prominent vascular remodeling with obliteration of the vessel lumen (Fig. 1a), and increased vessel wall thickness (Fig. 1b), consistent with prior reports.[2] Immunohistochemistry studies identified increased NAMPT expression in EC of pulmonary blood vessels quantified by Image J analyses (Fig. 1c and d). Similar findings was confirmed by Western blot for NAMPT concentration in lung homogenates in studied group, and showed significant increase in hypoxia/Sugen group, in comparison to both control and mAb-treated hypoxia/Sugen group (Fig. 1e and f). Delivery of an eNAMPT-neutralizing mAb beginning in week 4 (1 mg/kg, 2 times/week, IP), significantly reduced hypoxia/Sugen-mediated pulmonary vascular remodeling reflected by diminished pulmonary arterial

(PA) wall thicknesses in small (50 μm) and intermediate (100 μm) arteries (**Fig. 1b**). Thus, eNAMPT neutralization significantly attenuates vascular injury and remodeling in hypoxia/Sugen-induced experimental PH. We speculate the eNAMPT mAb-mediated reduction in NAMPT tissue expression reflects the attenuation of hypoxia/Sugen-induced inflammatory pathway activation.

eNAMPT neutralization attenuates hypoxia/Sugen-induced hemodynamic/echocardiographic PH abnormalities

The reduced vascular remodeling observed in eNAMPT mAb-treated PH rats was accompanied by significant attenuation of both hypoxia/Sugen-induced hemodynamic and echocardiographic abnormalities. Compared to room air (RA)-exposed controls, hemodynamic studies confirmed severe PH in hypoxia/Sugen-exposed rats with marked increases in right ventricular (RV) systolic pressure (RVSP), a surrogate measure of pulmonary arterial systolic pressure, and RV hypertrophy (RVH), reflected by
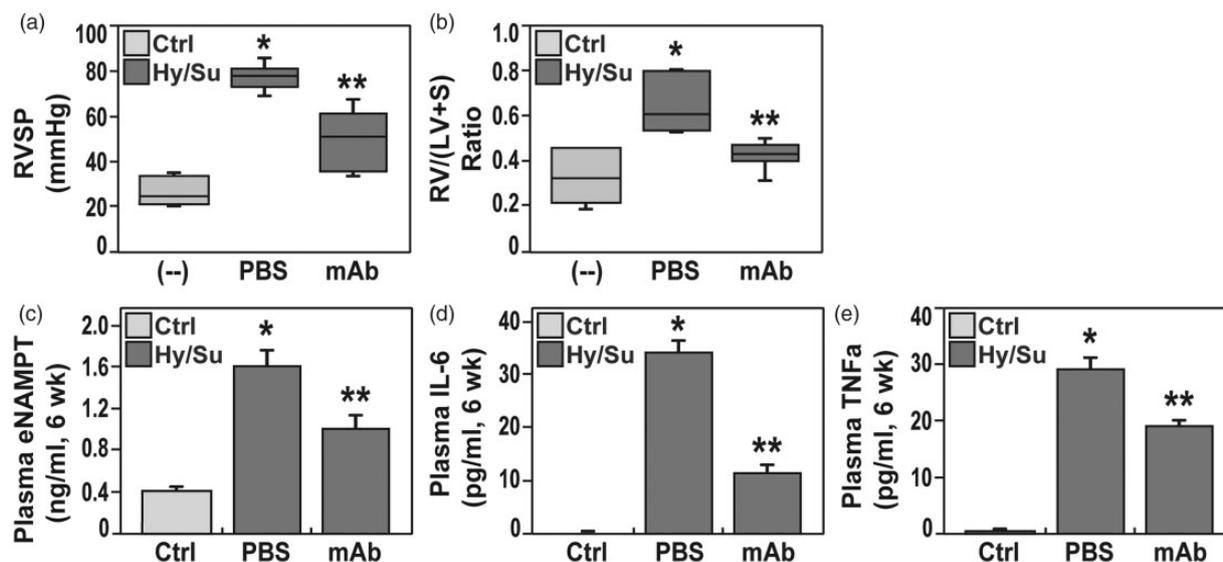
Figure 2. Boxplot depiction of right ventricular systolic pressure (RVP, Panel a) and right ventricular/left ventricle + septum ratio- (RV/LV+S, Panel b) in adult Sprague Dawley rats exposed to room air (control rats), to hypoxia/Sugen (three weeks hypoxia exposure, three weeks Sugen), and to hypoxia/Sugen while receiving IP delivery of eNAMPT mAb (1 mg/kg). Both hemodynamic parameters at six weeks were significantly elevated in hypoxia/Sugen-exposed rat group whereas rats treated with the eNAMPT-neutralizing mAb showed a significant reduction in both RVP and RV/LV+S in comparison to non-treated group. (c–e) Plasma levels of eNAMPT (c) Interleukin-6 or IL-6 (d), and TNF-α (e) were assessed in the three studied rat groups and revealed significant increases in each inflammatory mediator in hypoxia/Sugen-exposed rats compared with room air controls. Hypoxia/Sugen-exposed rats receiving the eNAMPT mAb exhibited marked reductions in each cytokine at six weeks. N= 5/ groups. Bars represents mean ± SE. *$p<0.05$ vs. RA controls; ** $p<0.05$ vs. hypoxia/Sugen-exposed untreated rats.

Table 1. Echocardiographic indices of right ventricular and cardiac function in preclinical rat PH.

	Control	Hypoxia/Sugen-PBS (wk 4 to 6, p= H/Su vs. RA)	Hypoxia/Sugen-mAb (wks 4 to 6)	p-value (H/Su vs. ALT)
Stroke volume (μL)	256.6 ± 34	170.6 ± 22 ($p = 0.01$)	250.8 ± 28	0.02*
Cardiac output (ml/min)	88.3 ± 5.3	60.4 ± 4.9 ($p = 0.002$)	84.4 ± 5.2	0.008*
RV ejection fraction	79.4 ± 4.3	57.7 ± 4.1 ($p = 0.01$)	73.8 ± 4.9	0.03*
Fractional shortening	43.3 ± 3.4	37.0 ± 3.5 ($p = 0.01$)	39.3 ± 4.1	0.8
Myocardial performance index	0.8 ± 0.06	1.3 ± .12 ($p = 0.01$)	0.9 ± .1	0.04*
RV fractional wall thickening	0.8 ± 0.08	1.7 ± 0.07 ($p = .0001$)	1.1 ± 0.08	0.03*
Pulmonary acceleration time	32.4 ± 3.8	16.5 ± 2.1 ($p = 0.001$)	28.4 ± 0.3.0	0.01*
PAT/PET	0.45 ± .05	0.2 ± 0.04 ($p = 0.001$)	0.4 ± 0.04	0.01*
TAPSE	1.1 ± 0.05	0.8 ± 0.03 ($p = 0.01$)	0.9 ± 0.03	0.04*

PAT: pulmonary acceleration time; PET: pulmonary ejection time; TAPSE: tricuspid annular plane systolic excursion.

alterations in the Fulton index, i.e. the ratio of the weight of RV to the weight of LV and septum (S) [RV/(LV+S)] (Fig. 2a and b). Each hypoxia/Sugen-mediated hemodynamic abnormality at six weeks was significantly normalized by eNAMPT mAb treatment initiated at week 4 (Fig. 2). Hemodynamic parameters in naïve, unexposed rats were comparable and without significant differences to the saline-injected control group (data not shown).

Echocardiographic indices were similarly abnormal in hypoxia/Sugen-exposed PH rats with dramatic increases in RV fractional wall thickening (RVFWT), a correlate of RV hypertrophy, and significant decreases in pulmonary acceleration time (PAT) and pulmonary ejection time (PAT/

PET), parameters that reflect RV afterload, and tricuspid annular plane systolic excursion (TAPSE) (Table 1). As with hypoxia/Sugen-induced vascular remodeling and hemodynamic abnormalities, eNAMPT mAb treatment (weeks 4 through 6) normalized RVFWT with reductions in both PAT and PAT/PET measurements (Table 1).

eNAMPT neutralization reduces circulating levels of eNAMPT, IL-6, and TNF-α

Consistent with the intimate relationship between inflammation and PAH outcomes[31–33] hypoxia/Sugen-exposed PH rats exhibited significant increases in plasma

eNAMPT, IL-6, and TNF-α levels at six weeks compared to RA controls (Fig. 2) with levels of each cytokine significantly attenuated by the eNAMPT mAb, indicating a reduction in overall inflammatory burden (Fig. 2c–e).

Hypoxia-induced PH abnormalities are attenuated in Nampt-engineered mice

To explore the specific contribution of EC-generated NAMPT in driving experimental PH, responses to 10% hypoxia for three weeks were compared in wild-type (WT) C57BL/6J mice, heterozygous $Nampt^{+/-}$ mice and conditional EC-targeted $cNampt^{ec-/-}$ KO mice. Compared to RA controls, hypoxia-exposed WT mice developed findings that were highly consistent with RV hypertrophy (RVH) including increased RVP (37.7 ± 2.6 mmHg vs. 12.5 ± 2.0 mmHg, respectively) with concomitant increases in the Fulton index (0.54 ± 0.04; vs. 0.22 ± 0.02, respectively), (Fig. 3a and b). These hemodynamic indices were significantly reduced in hypoxia-exposed $Nampt^{+/-}$ heterozygous mice and to a greater extent in $cNampt^{ec-/-}$ mice including RVSP (27.0 ± 2.3 mmHg; vs. 18.0 ± 2.1, respectively) and RV/LV + septum ratios (0.38 ± 0.04; vs. 0.28 ± 0.02 mmHg, respectively) (Fig. 3a and b). Echocardiographic studies with $cNampt^{ec-/-}$ mice confirmed dramatic normalization of RV fractional wall thickening, PAT, PAT/PET, and TAPSE (Table 2). Furthermore, $cNampt^{ec-/-}$ mice exhibited less severe vascular remodeling compared with WT hypoxia-exposed littermates (Fig. 3c and d). Hemodynamic parameters in naïve, unexposed rats were comparable and without significant differences to the saline-injected control group (data not shown).

SNAI1 is a transcription factor that regulates endothelial-to-mesenchymal transition (EndMT) known to participate in preclinical development of pulmonary vascular remodeling and hypertension.[4,12,34] Hypoxia-exposed WT mice demonstrated significant evidence of increased EndMT reflected by increased protein expression in lung homogenates of smooth muscle actin (SMA) and SNAI1 with reduced expression of CD31/PECAM (Fig. 3e–g). In contrast, compared to hypoxia-exposed WT mice, $cNampt^{ec-/-}$ mice exhibited near normalization fo the EndMT findings, results highly consistent with a role for EC-derived NAMPT in driving EndMT in experimental PH.

eNAMPT neutralization rectifies dysregulated rat PH genes and signaling pathways

Bioinformatic analyses of RNA sequencing of hypoxia/Sugen-exposed lung tissues were compared to RA rat controls utilizing a FDR <5% and a fold change (FC) of ± 1.5, yielding 122 differentially-expressed genes (DEGs) depicted in the heat map in Fig. 4a. DEGs were annotated for GO, KEGG, and REACTOME pathway analyses and STRING interactomes revealing "TNF," "AGE-RAGE," "HIF-1,"

and "MAP kinase family" as strongly dysregulated signaling pathways (Fig. 4b, Supplemental Table 1).

Similar comparisons between untreated and eNAMPT mAb-treated PH rats revealed a total of 60 DEGs (FDR 15%, 33 upregulated, 8 downregulated) with the most highly significant eNAMPT mAb-influenced GO Biologic Processes including "Chronic inflammatory response," "Lymphocyte and neutrophil chemotaxis," "Responses to IL-6," Interferon gamma and TNF," "Regulation of systemic arterial blood pressure," and "Chemokine signaling" (Fig. 4c and d, Supplemental Table 2).

Human PAH PBMCs exhibit dysregulated NFkB and TLR4 inflammatory pathways

Preclinical PH genomic results and the potential role of the eNAMPT/TLR4 pathway in human PAH were next validated by RNA sequencing and bioinformatic analyses of PBMC RNA from six normal subjects and six PAH subjects. PAH or control subject PBMCs were exposed *ex vivo* to either an IgG control or to the eNAMPT-neutralizing mAb (25 μg/mL, 6 h). The resulting 33 upregulated and 54 downregulated DEGs proved to organize into 8 GO-based clusters enriched in Toll-like receptor (TLR), NFkB, TNF-α, and IL-1β signaling pathways (Fig. 5a). Fig. 5b depicts the biological interactions among the 32 prioritized candidate DEGs with strong evidence of interaction among 18 of the 32 genes. The influence of eNAMPT/TLR4-mediated signaling in PAH subjects was not observed in control subjects, Details of the eNAMPT mAb-influenced clusters are in Supplemental Table 3.

eNAMPT neutralization rectifies dysregulated NFkB and Akt/mTORC2 signaling in rat PH

To validate genomic findings of preclinical PH-associated dysregulated signaling pathways, lung tissue homogenates were probed for NFkB and Akt/mTOR signaling proteins compared to control tissues. These studies revealed robust NFkB pathway activation, reflected by NFkB phosphorylation (Fig. 6a and b), and strong Akt/mTOR pathway dysregulation, reflected by reductions in Akt and mTOR protein levels (Fig. 6a, c and d). Protein levels of the mTORC2 cofactor, Rictor, were also reduced, whereas the mTORC1 cofactor, Raptor, was unaffected (Fig. 6a, d and e).

Consistent with EndMT findings in hypoxia-exposed WT mice and the known regulation of EndMT by Akt/mTOR, SNAI1 protein expression was increased in rat PH lung tissues but markedly rectified by the eNAMPT-neutralizing mAb (Fig. 6a and g). Finally, genomic dysregulation of HIF and MAP kinase family signaling pathways (Fig. 4) was strongly corroborated in biochemical studies demonstrating increased HIF-1α/HIF-2α expression and phosphorylation of ERK, p38, and JNK MAP kinases (Fig. 6a and h–l). Importantly, these hypoxia/Sugen-
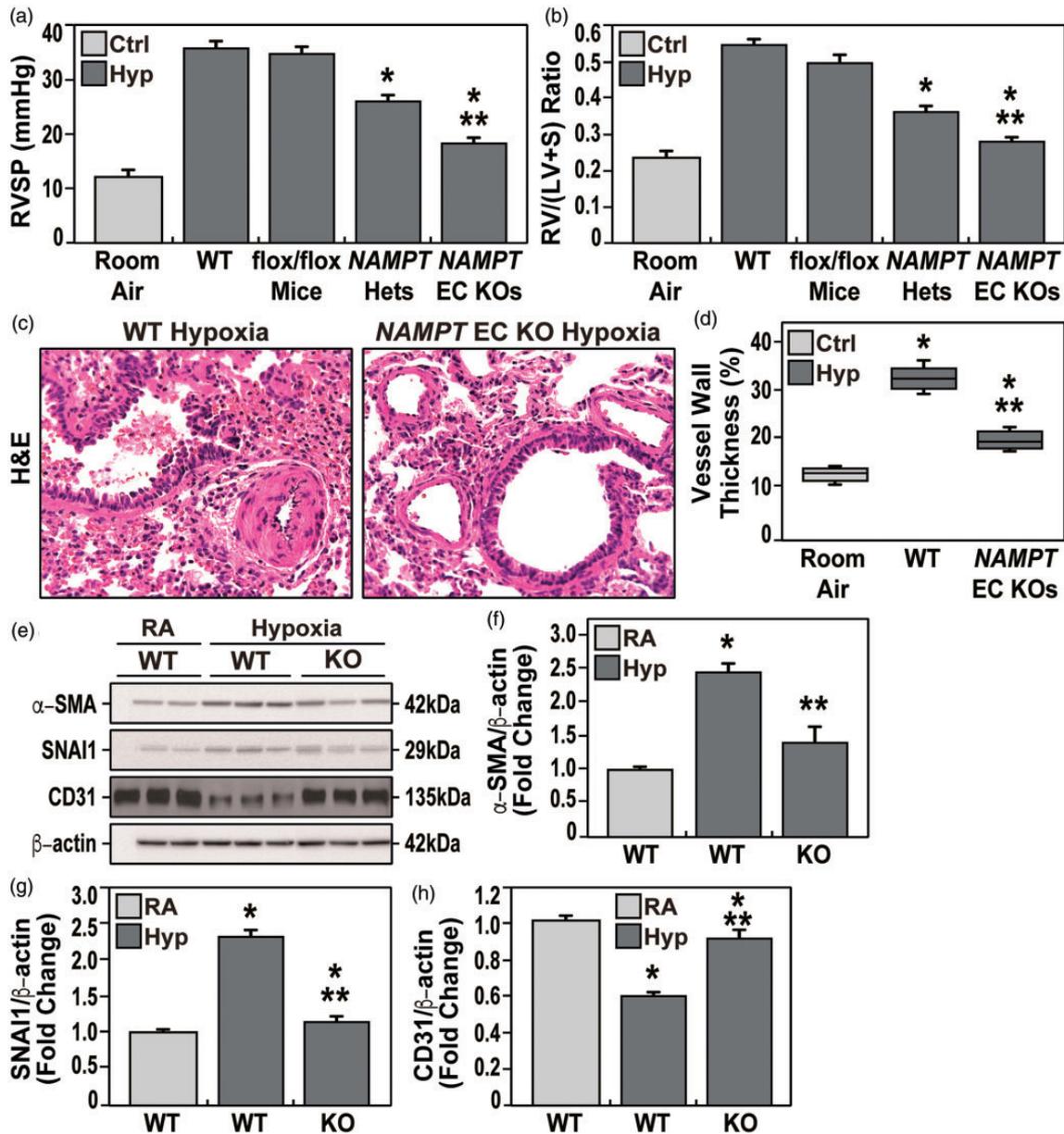
Figure 3. Evaluation of hemodynamic parameters in the three studied groups after three weeks of hypoxia exposure (FiO$_2$ 10%). a and b. Both mean right ventricular systolic pressure (RVP) and right ventricular/left ventricle + septum ratio (RV/LV+S) parameters were significantly lower in NAMPT$^{+/-}$ heterozygous mice and cNampt$^{ec-/-}$ mice compared to WT hypoxia-exposed mice. cNampt$^{ec-/-}$ mice also exhibited significantly lower RVP and RV/LV+S than Nampt$^{+/-}$ heterozygous mice and WT hypoxia-exposed mice. (c) Shown are the H&E lung sections of both hypoxia-exposed WT mice and cNampt$^{ec-/-}$ mice. WT mice showed a significant increase of vascular wall thickness due to muscular hypertrophy compared to KO mice which is comparable to RA control group. (d) Quantitative evaluation (boxplots) of the vascular wall thickness in hypoxia-exposed WT mice showed a significant increase of vascular wall thickness due to muscular hypertrophy compared to hypoxia-exposed cNampt$^{ec-/-}$ mice which is comparable to RA control group. Five sections/animal, N= 5/groups. Bars represents mean ± SE. *p<0.05, **p<0.01. n= 5/groups. Bars represents mean ± SE. *p<0.05, **p<0.01. (e–h) Western blots of immunoreactive proteins in lung homogenates (e) from room air-exposed WT mice and hypoxia-exposed WT and cNampt$^{ec-/-}$ mice with densitometric quantification of protein levels of a-smooth muscle actin (SMA) (f), SNAI1 (g), and CD31/PECAM (h). These studies show hypoxia-induced increases in SMA and SNAI and reduced PECAM expression, each finding consistent with enhanced EndMT. Each index of EndMT activation were significantly attenuated in cNampt$^{ec-/-}$ mice.

mediated dysregulated pathways were rectified by the eNAMPT mAb indicating the high feasibility of targeting the eNAMPT/TLR4 inflammatory signaling pathway to slow progression or reverse PAH pathobiology.

Discussion

In stark contrast to a focus on iNAMPT enzymatic function, we have detailed the novel participation of secreted

Table 2. Hypoxia-induced echocardiographic changes in wild-type and endothelial cell-conditional *NAMPT* KO mice.

	Room air WT vs. Namptec$^{-/-}$ Mice	Wild-type mice (Hypoxia, 3 wk)	cNamptec$^{-/-}$ mice (Hypoxia, 3 wk)	p-value
Stroke volume (μL)	36.2 ± 3.4 vs. 35.6 ± 3.2	32.2 ± 2.4	33.8 ± 3.2	NS
Cardiac output (ml/min)	17.1 ± 2.4 vs. 16.2 ± 2.2	15.8 ± 2.1	14.5 ± 1.8	NS
Ejection fraction	65.5 ± 5.1 vs. 58.2 ± 5.6	41.2 ± 4.2	51.4 ± 3.8	$p < 0.05$
Myocardial performance index	16 ± 1.6 vs. 16 ± 1.8	18 ± 1.4	17 ± 1.2	NS
RV fractional wall thickening	$0.31 \pm$ vs. 0.3	0.53	0.36	$p < 0.05$
Pulmonary acceleration time	$20 \pm$ vs. 17.2	13.5	17.5	$p < 0.05$
PAT/PET	$0.36 \pm$ vs. 0.35	0.27	0.34	$p < 0.05$
TAPSE	1.02 vs. 0.99	0.7	0.94	$p < 0.05$

PAT: pulmonary acceleration time; PET: pulmonary ejection time; TAPSE: tricuspid annular plane systolic excursion.
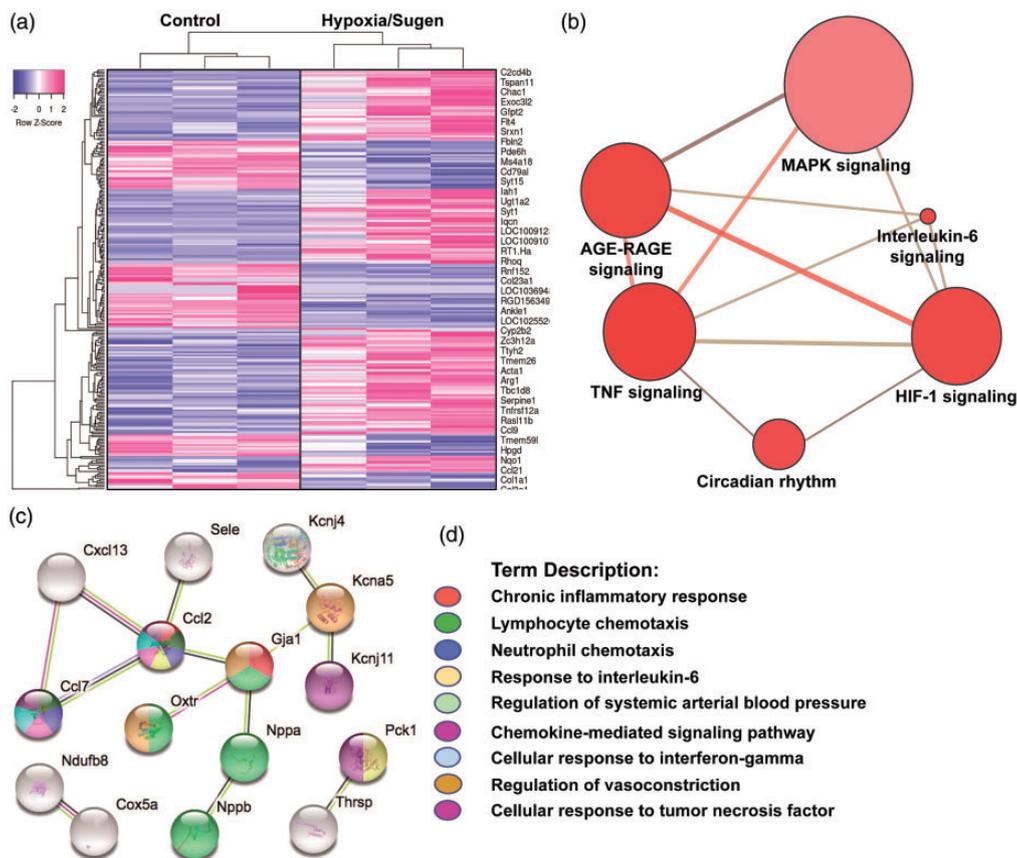

Figure 4. eNAMPT neutralization attenuates hypoxia/Sugen-induced PH dysregulated genes and signaling pathways. A total of 122 prioritized DEGs (81 upregulated and 31 downregulated) were identified by comparison of genomic responses of hypoxia/Sugen-exposed rats with room air control rats at six weeks. A corrected *p*-value of less than 0.05 (Fisher exact test BH method) and a FC >1.5 and <1.5 were considered. (a) Heat map depicting the top upregulated and downregulated DEGs selected from comparisons of RNA sequencing data from hypoxia/Sugen and RA controls. Gene expression values are represented by the z-score. (b) Visualization of the functional annotation of the pathway-based sets derived from the DEGs. The size of the bubble reflects the number of genes in that pathway and the red intensity reflects the *p* value magnitude with darker red being increasing *p* value. The top KEGG and Reactome functional pathways associated terms are further detailed in Supplement Table 1. (c and d) Bioinformatic analysis of RNA sequencing data from hypoxia/Sugen-exposed rats that were influenced by eNAMPT mAb treatment revealed a total of 60 DEGs (*p*-adjusted value <0.15) with prioritized DEGs depicted in a STRING network analysis for GO terms. The colors denote the associated GO Biologic Processes (FDR of <0.02) with network elements. Additional eNAMPT-influenced pathways utilizing consensus (KEGG and Reactome) databases are detailed in Supplement Table 2.
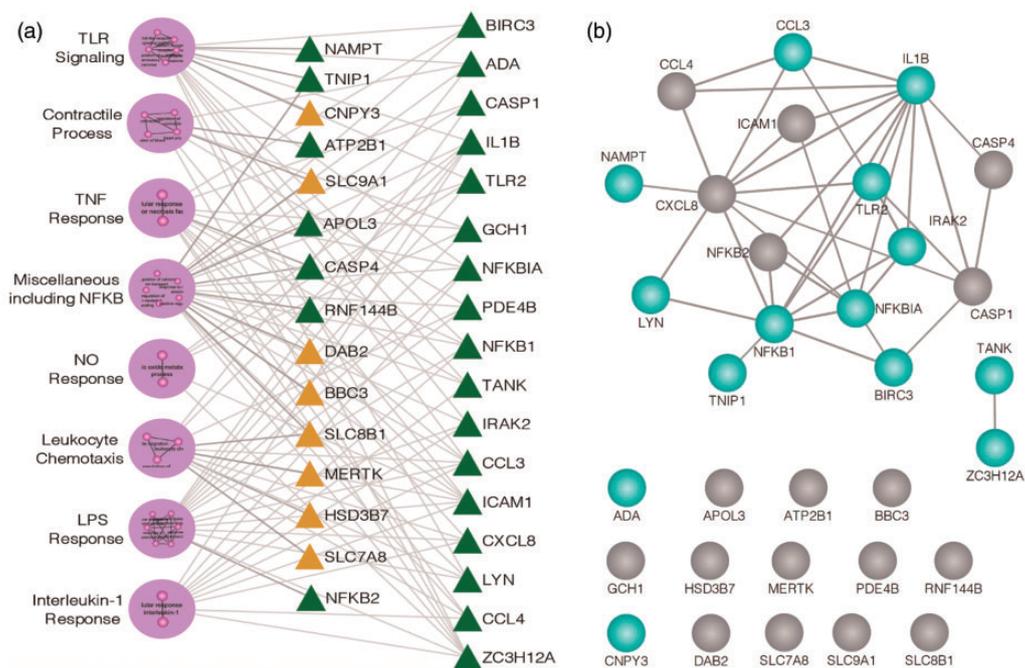
Figure 5. Human PAH PBMCs show basal Toll-like Receptor (TLR) pathway/gene dysregulation: rectification by eNAMPT-neutralizing mAb. (a) RNAseq was performed in PBMCs from six PAH subjects compared to six control subjects incubated (6 h) with and without ALT-100 eNAMPT-neutralizing mAb. 87 DEGs (54 downregulated, 33 upregulated) were prioritized reflecting the influence of the eNAMPT-neutralizing mAb (BH corrected $p < 0.05$). A total of 29 GO-based biologic processes (GOBP) were inferred (BH p-value of Fisher's exact test < 0.05). Shown are the eight clusters of highly similar biological processes with green triangles reflecting genes downregulated by eNAMPT mAb exposure and yellow triangles signifying upregulated genes. Clusters are further detailed in Supplement Table 3. (b) STRING (Version 11) was employed to characterize the biological interaction among the 32 candidate genes providing strong evidence for interaction among 18 out of 32 genes especially for TLR signaling transcripts highlighted in blue. The remaining 14 genes were not observed with pairwise interactions in STRING.

eNAMPT as a novel DAMP via binding of the pathogen-recognition receptor, TLR4,[6] to drive the severity of human inflammatory lung disorders with unmet therapeutic needs such as sepsis/ARDS,[35,36] ventilator-induced lung injury,[9,10] and, more recently, chronic diseases such as prostate cancer[37] and PAH.[3,4] We reported eNAMPT generation and secretion are increased by diverse PAH-relevant stimuli such as PDGF, VEGF, TGF-β1, and hypoxia,[4] by mechanical stress,[9] and by both bacterial and viral infections including SARS-CoV2.[5,35] Initial studies linking NAMPT to PAH pathobiology demonstrated increased *NAMPT* RNA and protein expression in human PAH and murine/rat PH vascular cells.[3,4] Plasma levels of eNAMPT are elevated in PAH subjects and correlate with RV diastolic dysfunction.[4] Monocrotaline-induced PH rat studies demonstrated a polyclonal eNAMPT-neutralizing Ab to reduce RV dysfunction and vascular remodeling in PAH lung vessels.[4] These results are consistent with prior studies examining the role of eNAMPT in the development of cardiac hypertrophy and ventricular remodeling where the hypertrophic response was blunted in *Nampt*^{+/−} heterozygous and cardiac-specific overexpressing *Nampt* transgenic mice spontaneously developed cardiac hypertrophy which was blocked by a polyclonal eNAMPT-neutralizing antibody.[38]

The current study extends these earlier PAH reports in two highly impactful ways. First, our study design is differentiated from commonly utilized experimental designs focused on prevention. We now demonstrate the unequivocal therapeutic benefits of eNAMPT mAb delivery (beginning in week 4) to rats with established PH. Our studies detail the significant attenuation of RV dysfunction confirmed by echocardiographic studies, physiologic improvements reflecting eNAMPT mAb-mediated reductions in pulmonary vascular resistance and progressive vascular remodeling. Our rat and human genomic studies strongly highlight direct involvement of eNAMPT/TLR4 and NFkB inflammatory signaling in PAH, and dramatically underscore the feasibility of therapeutically targeting the eNAMPT/TLR4 signaling to effectively halt PAH progression and potentially reverse PAH processes.

An absolutely key extension of the current work over prior reports is the clear delineation of the influence of EC-specific NAMPT expression and secretion in experimental PH. We previously showed increased EC-derived NAMPT expression within human and rodent PAH pulmonary vessels; however, the role of cell-specific NAMPT expression was unknown. Utilizing EC-specific conditional *cNampt*[ec−/−] mice, we now convincingly demonstrate that EC-specific NAMPT expression directly contributes to
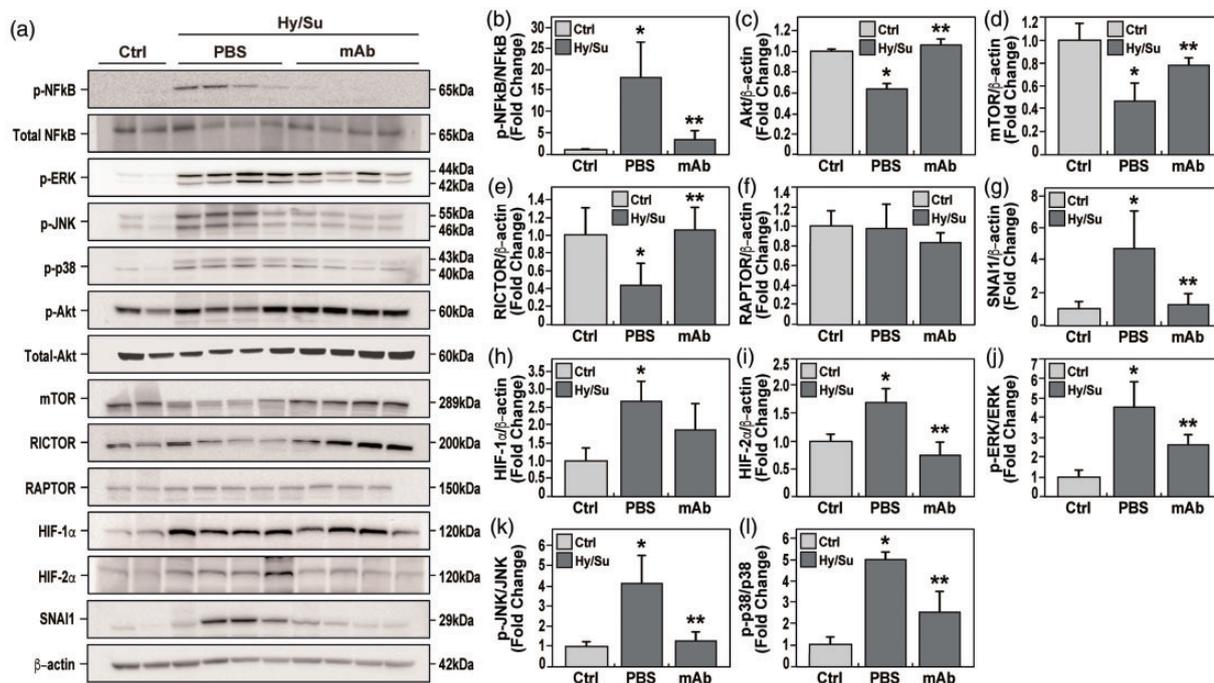
Figure 6. eNAMPT neutralization attenuates hypoxia/Sugen-induced PAH dysregulated signaling proteins and pathways. (a) Western blotting studies were conducted for major signaling proteins in lung tissue homogenates obtained at six weeks from room air control rats (lanes 1 and 2), untreated hypoxia/Sugen-exposed rats (lanes 3–6), and eNAMPT mAb-treated hypoxia/Sugen-exposed rats (lanes 7–10). For each protein, densitometric results confirmed prominent hypoxia/Sugen-induced alterations in protein levels with each altered protein expression markedly reduced in hypoxia/Sugen-exposed rats receiving the eNAMPT-neutralizing mAb (1 mg/kg, 2×/week). These include the ratio of p-NFkB/NFkB (fold change) (a and b), and proteins intrinsic to the Akt/mTOR pathway with hypoxia/Sugen-induced loss of total protein including Akt (c), mTOR (d) and Rictor (e) whereas Raptor was unaffected (f). Hypoxia/Sugen-induced alterations of NFkB and Akt pathway proteins inhibited or abolished in rats receiving the eNAMPT-neutralizing mAb. Biochemical evaluation of lung homogenate for the EndMT inducer, SNAI1, revealed hypoxia/Sugen-induced increases SNAI1 (g) as well as the HIF transcription factor, HIF-1α and HIF-2α (h and i) which were normalized in rats receiving the eNAMPT-neutralizing mAb. Finally, the hypoxia/Sugen-induced activation of the MAP kinase family proteins with increases in p-ERK/ERK (j), p-JNK/JNK (k), p-p38/p-38 (l) was also normalized in rats receiving the eNAMPT-neutralizing mAb.

preclinical PH severity with nearly normalization of multiple indices of hypoxia-induced PH severity (vascular remodeling, hemodynamic/echocardiographic parameters). Our studies also provide a mechanistic basis for the influence of DAMPs, such as eNAMPT, and for pathogen-recognition receptors, such as TLR4, on PAH pathologic processes such as lung EndMT that promote vascular remodeling and occlusive lesions.[12] Our combined studies in *cNampt*[ec−/−] mice and in eNAMPT mAb-treated PH rats detail the generation of eNAMPT by EC as vital to EndMT development and PH severity with attenuated expression of SNAI1, a member of the SNAI family of zinc-finger transcription factors and known EndMT inducer and driver.[4,12,34] These findings of eNAMPT-enhanced EndMT are highly consistent with our prior *in vitro* demonstration in human lung endothelium of direct eNAMPT-mediated increases in SNAI1 expression, reductions in PECAM expression, and increases in discontinuous adherens junction staining.[4] As we recently reported that HIF-2α markedly increases *NAMPT* transcription, accelerates eNAMPT secretion,[4] and increases EC expression of SNAI1,[4,12] our current studies provide for a potential mechanism for HIF-2α effects on PAH development via EC

eNAMPT generation, EndMT, and progressive pulmonary vascular remodeling and occlusive lesions.[4,12]

Our speculated mechanism of action entails eNAMPT-induced TLR4 signing to promote vascular wall thickness by enhancing endothelial-to-mesenchymal transition. eNAMPT-treated EC exhibit increased expression of the EndMT transcription factor, SNAI1 (EndMT driver), significantly decreased PECAM1 expression (EC marker) and significantly increased discontinuous adherens junction.[4] Combined with the prominent fibrosis-enhancing effects of eNAMPT we have observed in cardiac and pulmonary fibrosis,[38,39] these data support the mechanistic contribution of eNAMPT in the pathobiology of PAH.

The Akt/mammalian target of rapamycin (mTOR) signaling cascade is critically involved in PH development and commitment of ECs to enter EndMT. Akt signaling is activated by various PAH-relevant growth factors, mitogenic cytokines, endothelin-1, stress, and hypoxia.[34] Deletion of the *Akt1* gene in mice significantly inhibits development of experimental PH[25] and the knockout of Rictor (rapamycin-insensitive companion of mTOR), which functionally disrupts the formation of the mTORC2 complex, results in spontaneous PH.[34] In contrast, the knockout of Raptor

(regulatory associated mTOR protein) to functionally disrupt mTORC1, served to ameliorate experimental PH.[34] Our biochemical results underscore the strong hypoxia/Sugen-mediated dysregulation of the Akt/mTOR/Rictor pathway reflected by reductions in lung tissue levels of Akt, mTOR, and Rictor whereas Raptor protein levels were unaffected. Importantly, in addition to Akt/mTORC2/Rictor, each PH dysregulated signaling pathway, including NFkB, HIF, and MAP kinase family, was markedly rectified in rats receiving the eNAMPT mAb at week 4.

In summary, given the linkage between innate immunity and inflammatory cytokines to PAH severity and survival,[31–33,40–43] our studies underscore the importance of endothelial cell generation of the DAMP, eNAMPT, and its binding to the pathogen-recognition receptor, TLR4, in driving the development and severity of experimental PH. Our results with a humanized eNAMPT-neutralizing mAb demonstrate eNAMPT/TLR4 as a highly druggable PAH target to halt or reverse multiple hemodynamic, echocardiographic, and vascular remodeling indices of severe experimental PH. Genomic and biochemical approaches in both rat lung tissues and in human PAH PBMCs, linked eNAMPT/TLR4 signaling to dysregulation of signaling pathways that contribute to EndMT and to PAH development. Thus, in addition to addressing a serious unmet PAH for novel therapeutics, these studies provide novel molecular insights into the interface between inflammation, innate immunity, and PAH pathogenesis.

Conflict of interest

Funding

Authors' contribution

JGNG, MA – Conception and design of the work, the analysis and interpretation of data for the work, the drafting and revision of the manuscript, approval of final version to be published; NGC, AAD, YL, AM, FR, JW, JXJY – Conception and design of the work, the analysis and interpretation of data for the work, critical revision of key intellectual content and approval of final version to be published; SMC, CLK, RCO, OR, RR, SS, XS – Collection and analysis of data, revision of the manuscript, and approval of the final version to be published; VRH, NZ, PZ – Collected data and assisted with processing and manuscript revision.

ORCID iDs

Ayako Makino https://orcid.org/0000-0003-1259-8604
Sara M. Camp https://orcid.org/0000-0001-5521-9841
Jason X.-J. Yuan https://orcid.org/0000-0002-0685-4862
Joe G.N. Garcia https://orcid.org/0000-0002-6934-0420

Supplemental Material

Supplementary material for this article is available online.

References

1. Girgis RE, Ma SF, Ye S, et al. Differential gene expression in chronic hypoxic pulmonary hypertension: effect of simvastatin treatment. *Chest* 2005; 128: 579S.
2. Moreno-Vinasco L, Gomberg-Maitland M, Maitland ML, et al. Genomic assessment of a multikinase inhibitor, sorafenib, in a rodent model of pulmonary hypertension. *Physiol Genom* 2008; 33: 278–291.
3. Chen J, Sysol JR, Singla S, et al. Nicotinamide phosphoribosyltransferase promotes pulmonary vascular remodeling and is a therapeutic target in pulmonary arterial hypertension. *Circulation* 2017; 135: 1532–1546.
4. Sun X, Sun BL, Babicheva A, et al. Direct extracellular NAMPT involvement in pulmonary hypertension and vascular remodeling. transcriptional regulation by SOX and HIF-2alpha. *Am J Respir Cell Mol Biol* 2020; 63: 92–103.
5. Bime C, Casanova NG, Nikolich-Zugich J, et al. Strategies to DAMPen COVID-19-mediated lung and systemic inflammation and vascular injury. *Transl Res* 2020: S1931.
6. Camp SM, Ceco E, Evenoski CL, et al. Unique toll-like receptor 4 activation by NAMPT/PBEF induces NFkappaB signaling and inflammatory lung injury. *Sci Rep* 2015; 5: 13135.
7. Garten A, Schuster S, Penke M, et al. Physiological and pathophysiological roles of NAMPT and NAD metabolism. *Nat Rev Endocrinol* 2015; 11: 535–546.
8. Oita RC, Camp SM, Ma W, et al. Novel mechanism for nicotinamide phosphoribosyltransferase inhibition of TNF-alpha-mediated apoptosis in human lung endothelial cells. *Am J Respir Cell Mol Biol* 2018; 59: 36–44.
9. Hong SB, Huang Y, Moreno-Vinasco L, et al. Essential role of pre-B-cell colony enhancing factor in ventilator-induced lung injury. *Am J Respir Crit Care Med* 2008; 178: 605–617.
10. Quijada H, Bermudez T, Kempf CL, et al. Endothelial eNAMPT amplifies preclinical acute lung injury: efficacy of an eNAMPT-neutralising mAb. *Eur Respir J* 2020: 2002536.
11. Korhonen H, Fisslthaler B, Moers A, et al. Anaphylactic shock depends on endothelial Gq/G11. *J Exp Med* 2009; 206: 411–420.
12. Tang H, Babicheva A, McDermott KM, et al. Endothelial HIF-2alpha contributes to severe pulmonary hypertension due to endothelial-to-mesenchymal transition. *Am J Physiol Lung Cell Mol Physiol* 2018; 314: L256–L275.
13. Bellofiore A, Vanderpool R, Brewis MJ, et al. A novel single-beat approach to assess right ventricular systolic function. *J Appl Physiol (1985)* 2018; 124: 283–290.
14. Heerdt PM, Kheyfets V, Charania S, et al. A pressure-based single beat method for estimation of right ventricular ejection fraction: proof of concept. *Eur Respir J* 2020; 55: 1901635.
15. Ahmed MN, Zhang Y, Codipilly C, et al. Extracellular superoxide dismutase overexpression can reverse the course of hypoxia-induced pulmonary hypertension. *Mol Med* 2012; 18: 38–46.

16. Tarazona S, Furio-Tari P, Turra D, et al. Data quality aware analysis of differential expression in RNA-seq with NOISeq R/Bioc package. *Nucleic Acids Res* 2015; 43: e140.
17. Langmead B and Salzberg SL. Fast gapped-read alignment with Bowtie 2. *Nat Methods* 2012; 9: 357–359.
18. Law CW, Chen Y, Shi W, et al. voom: precision weights unlock linear model analysis tools for RNA-seq read counts. *Genome Biol* 2014; 15: R29.
19. Liu R, Holik AZ, Su S, et al. Why weight? Modelling sample and observational level variability improves power in RNA-seq analyses. *Nucleic Acids Res* 2015; 43: e97.
20. Nueda MJ, Ferrer A and Conesa A. ARSyN: a method for the identification and removal of systematic noise in multifactorial time course microarray experiments. *Biostatistics* 2012; 13: 553–566.
21. Pertea M, Kim D, Pertea GM, et al. Transcript-level expression analysis of RNA-seq experiments with HISAT, StringTie and Ballgown. *Nat Protoc* 2016; 11: 1650–1667.
22. Ritchie ME, Diyagama D, Neilson J, et al. Empirical array quality weights in the analysis of microarray data. *BMC Bioinformatics* 2006; 7: 261.
23. Ritchie ME, Phipson B, Wu D, et al. limma powers differential expression analyses for RNA-sequencing and microarray studies. *Nucleic Acids Res* 2015; 43: e47.
24. Smyth GK. Linear models and empirical Bayes methods for assessing differential expression in microarray experiments. *Stat Appl Genet Mol Biol* 2004; 3: Article3.
25. Szklarczyk D, Gable AL, Lyon D, et al. STRING v11: protein-protein association networks with increased coverage, supporting functional discovery in genome-wide experimental datasets. *Nucleic Acids Res* 2019; 47: D607–D613..
26. Tarazona S, Garcia-Alcalde F, Dopazo J, et al. Differential expression in RNA-seq: a matter of depth. *Genome Res* 2011; 21: 2213–2223.
27. Benjamini Y and Hochberg Y. Controlling the false discovery rate: a practical and powerful approach to multiple testing. *J R Stat Soc* 1995; 57: 289–300.
28. Tao Y, Sam L, Li J, et al. Information theory applied to the sparse gene ontology annotation network to predict novel gene function. *Bioinformatics* 2007; 23: i529–i538.
29. Kim D, Langmead B and Salzberg SL. HISAT: a fast spliced aligner with low memory requirements. *Nat Methods* 2015; 12: 357–360.
30. Cock PJ, Fields CJ, Goto N, et al. The Sanger FASTQ file format for sequences with quality scores, and the Solexa/Illumina FASTQ variants. *Nucleic Acids Res* 2010; 38: 1767–1771.
31. Hassoun PM, Mouthon L, Barbera JA, et al. Inflammation, growth factors, and pulmonary vascular remodeling. *J Am Coll Cardiol* 2009; 54: S10–S19.
32. Rabinovitch M, Guignabert C, Humbert M, et al. Inflammation and immunity in the pathogenesis of pulmonary arterial hypertension. *Circ Res* 2014; 115: 165–175.
33. Pullamsetti SS, Savai R, Janssen W, et al. Inflammation, immunological reaction and role of infection in pulmonary hypertension. *Clin Microbiol Infect* 2011; 17: 7–14.
34. Tang H, Wu K, Wang J, et al. Pathogenic role of mTORC1 and mTORC2 in pulmonary hypertension. *JACC Basic Transl Sci* 2018; 3: 744–762.
35. Bime C, Casanova N, Oita RC, et al. Development of a biomarker mortality risk model in acute respiratory distress syndrome. *Crit Care* 2019; 23: 410.
36. Ye SQ, Simon BA, Maloney JP, et al. Pre-B-cell colony-enhancing factor as a potential novel biomarker in acute lung injury. *Am J Respir Crit Care Med* 2005; 171: 361–370.
37. Sun BL, Sun X, Casanova N, et al. Role of secreted extracellular nicotinamide phosphoribosyltransferase (eNAMPT) in prostate cancer progression: novel biomarker and therapeutic target. *EBioMedicine* 2020; 61: 103059.
38. Pillai VB, Sundaresan NR, Kim G, et al. Nampt secreted from cardiomyocytes promotes development of cardiac hypertrophy and adverse ventricular remodeling. *Am J Physiol Heart Circ Physiol* 2013; 304: H415–H426.
39. Garcia AN, Casanova NG, Valera DG, et al. Involvement of eNAMPT/TLR4 signaling in murine radiation pneumonitis: protection by eNAMPT neutralization. *Transl Res*. EPub ahead of print 18 June 2021. PMID: 34139379. DOI: 10.1016/j.trsl.2021.06.002.
40. Wang J, Tian XT, Peng Z, et al. HMGB1/TLR4 promotes hypoxic pulmonary hypertension via suppressing BMPR2 signaling. *Vasc Pharmacol* 2019; 117: 35–44.
41. Xiao G, Zhuang W, Wang T, et al. Transcriptomic analysis identifies Toll-like and Nod-like pathways and necroptosis in pulmonary arterial hypertension. *J Cell Mol Med* 2020; 24: 11409–11421.
42. Young KC, Hussein SM, Dadiz R, et al. Toll-like receptor 4-deficient mice are resistant to chronic hypoxia-induced pulmonary hypertension. *Exp Lung Res* 2010; 36: 111–119.
43. Soon E, Holmes AM, Treacy CM, et al. Elevated levels of inflammatory cytokines predict survival in idiopathic and familial pulmonary arterial hypertension. *Circulation* 2010; 122: 920–927.